Korean J. Chem. Eng., 40(12), 2847-2854 (2023)
DOI: 10.1007/s11814-023-1556-2

pISSN: 0256-1115
eISSN: 1975-7220

Interface engineering for enhancing the performance of novel sodium-doped MoS_2 nanocomposite: Synthesis and characterization functioning as a high-performance supercapacitor

Yedluri Anil Kumar*, Dasha Kumar Kulurumotlakatla, and Il-Kyu Park***,†**

*Department of Chemical & Petroleum Engineering, United Arab Emirates University (UAEU), Al Ain 15551, United Arab Emirates
**Graduate School of Convergence Science, Pusan National University, San 30 Jangjeon-dong, Geumjeong-gu, Busan 46241, Korea
***Department of Materials Science and Engineering, Seoul National University of Science and Technology, Seoul 01811, Korea

(*Received 1 August 2023 • Revised 15 August 2023 • Accepted 18 August 2023*)

Abstract−Novel structured Na-doped MoS_2 nanosheets were developed in situ on Ni foam through a more accessible two-step hydrothermal technique. Benefiting from the synergistic reactions of the superior capacitance of Na-doped MoS_2 nanosheet, the superior electrical kinetics of Na-doped, and the porous nanostructure of the composites, the designed Na-doped MoS_2 nanosheet composites electrode achieves notable electrochemical activity. The material's structural properties investigate using an X-ray photoelectron spectroscope analyzer, X-ray powder diffractions, scanning electron microscope, and transmission electron microscope. The electrochemical activity of the designed electrodes was executed using cyclic voltammograms, galvanostatic charge/discharges, and electrochemical impedance spectroscopy. Compared to the pure MoS_2 electrode, the novel architecture Na-doped MoS_2 nanosheet deremonstrates a higher specific capacity of 374.3 C g^{-1} at 1 A g^{-1}. In addition, it achieves notable cycling stability performance and retains 87.4% capacity over 5,000 long cycles at 3 A g^{-1}. These notable results reveal that the uniquely designed Na-doped MoS_2 nanosheet displays superior electrochemical consequences and higher potential as nanomaterials for supercapacitors.

Keywords: Na-doped MoS_2, Layered, Electrode Materials, Supercapacitors, Energy Storage

INTRODUCTION

In current scenarios, energy complications are supervening substantial issues and enthralling global consciousness. It's witnessed to be a crucial task for researchers to find new electrodes with higher performance in energy storage, conversions, and utilizations [1-3]. Supercapacitors (SCs) possess a new energy-storing cell that has a wide variety of advantages, such as a longer stability, greater power density, higher energy density, and greener eco-protection, and has attracted substantial academic interest in the past decades [4,5]. Compared with other energy storage devices, SCs provide much greater reasonable energy density (per unit masses) and power efficiency, rapid charge-discharge, and extended life span even in critical scenarios [6-9]. Supplementing the battery, SCs consist of initiating practical devices in faster switching, portable devices, backup energy providers, regenerative brake setup, motor vehicles, and factory energy/power purposes [10,11].

Carbon-type electrodes were typically utilized as samples in electrochemical double-layer capacitors (EDLCs) because of their notable longer-span electrochemical performance as an outcome of more excellent electrical kinetics and outstanding chemical conductivity, including carbon nanotubes, activated carbon, porous carbon, and carbide-procured graphene [9-12]. P-category doping was a considerable challenge for transition-metal dichalcogenides-typed SCs designs [12,13]. To enhance the p-based electrical characterizations of the electrodes, doping by group-I and V elements has been investigated by a few researchers. Na doping into transition-metal dichalcogenides has become engaging for a few scientists since it has theoretically assumed that Na ions substitute transition-metal dichalcogenides ions and form shallowed acceptor states [13-15]. Moreover, conquering the oxygens vacancies using Na was a significant path to fulfill lasting p-base conductivities [16-19]. Meanwhile, Na ions were anticipated to settle, acting as a donor [19]. On the other hand, Yuan et al. design of the group I atoms might be occupying the interstitial donor because of their smaller atomic radius, but the same interstitial sites impurities with Na dope can be impossible to supply because of its ionic radius compared to transition-metal dichalcogenides [18]. Particularly in SCs, it is crucial to find what the morphological and structural characteristics of transition-metal dichalcogenides are forced by [20]. Therefore, works to recognize the properties of sodium in transition-metal dichalcogenides are crucial. There are most works in the studies on Na-doped transition-metal dichalcogenides. Nevertheless, many studies in the report are usually narrow in scope. The consequences

†To whom correspondence should be addressed.
E-mail: pik@seoultech.ac.kr

of sodium dope on the limited characteristics of transition-metal dichalcogenides are much discussed, but the interrelationships of the reactions of Na dope on various behaviors are not yet considerable enough.

Layer-constructions transition-metal dichalcogenides, including molybdenum disulfide (MoS_2) and tungsten sulfide (WS_2), gained much attention due to their novel physical and chemical characterizations. Among considerable members, MoS_2 has the most attention in most fields, such as catalysis, electrochemical cells, solid lubricant, capacitors, hydrogen storage, and international hosts [21-23]. It consists of analogous graphite architectures composed of three atomic layers: a Mo-layered sandwich among two S-layers, with the third layer stacked and grouped together through weaker van-der-Waals interaction [24]. Recently, a capacitor study was also centered on MoS_2 predominantly because of its great intrinsic rapid ionic conductivity (than oxide types) and greater theoretical capacity (than carbon types) [25-27]. Soon et al. designed that MoS_2 is utilized as a sample for capacitors because of its sheets-type morphology, which offers larger specific regions for EDLCs charge storing [28]. The outcomes demonstrated that the SCs activity of MoS_2 was compared to graphite nanowire array materials. Moreover, capacitance of EDLCs, and ion diffusion into the MoS_2 at lesser scans surge to faradaic capacitances that significantly improve charge storing capacity. Nevertheless, the MoS_2 electronic conductivity was still limited comparable with graphite/Na-doped, and the specific capacity of MoS_2 was still lower for SCs devices. The combination of Na-dope and MoS_2 would overcome these deficiencies.

In this study, for the first time, we designed a unique nanosheet-type structure, Na-doped MoS_2 acquired from the overlapped or coalesced layers of Na-doped MoS_2 utilized as a unique electrode material for SCs. The Na-doped MoS_2 nanosheet improved the electrochemical characterization, indicating higher energy density for electrochemical SCs applications. The Na-doped MoS_2 nanosheet-based materials are detected to provide a capacity of 374.3 C g^{-1} at a 1 A g^{-1} with notable cycle stability over 5,000 long-run cycles in 2 M KOH electrolyte solution.

EXPERIMENTAL

1. Synthesis of MoS_2 Nanoparticles Grown on Ni Foam

MoS_2 nanoparticles were prepared by using the following process. 4.1 g of $Na_2MoO_4{\cdot}2H_2O$ (99.99%, Sigma-Aldrich) and 3.9 g of H_2NCSNH_2 (98%, Daejung Chemicals & Metals) were dissolved in 90 mL DI water and stirred for approximately 25 minutes. The pH value was then adjusted to less than 1 with the addition of 9 M of HCl (Daejung Chemicals & Metals), and the resulting mixture was transferred to a 120 mL autoclave and heated at 180 °C for 16 hours. Following this, the black-colored MoS_2 product was obtained by filtration and washed several times with DI water and pure ethanol before being dried in an oven at 70 °C for 17 hours.

2. Synthesis of Na-doped MoS_2 Nanosheet Developed on Ni Foam

The process for producing Na-doped MoS_2 nanosheets involved a hydrothermal method. 0.1 g of sodium nitrate dopant and 50 mL of water were added into the 200 mL vessel, followed by adding 0.5 g of MoS_2 precursor, which was stirred for 25 minutes. The pH value of the mixture was adjusted to 6.5 using 0.2 M of NaOH. The final product mixture was transferred to a 150 mL autoclave containing 120 mL of DI water and then heated to 140 °C for 32 hours. After cooling to room temperature, the black precipitates of Na-doped MoS_2 composites were collected by centrifugation, washed with DI water and ethanol, and dried in a vacuum oven at 90 °C for 16 hours.

3. Characterization and Instruments

The compositional crystal constructions of the electrodes were analyzed using X-ray diffraction (XRD, Bruker D8 Advance) at 2θ scopings of 20-80°. The microscopic and morphological identification of the electrodes was detected using a scanning electron microscope (SEM; JSM-7800F). A transmission electron microscope (TEM; JEM-2100F) was taken to examine the electrode's internal structure. The elemental compositions and chemical valence states of the nanomaterials were analyzed using an X-ray photoelectron spectroscope (XPS; ESCALAB 250Xi).

4. Electrochemical Performance Test

Electrochemical calculations are managed on a Bio-Logical electrochemical work-station. The designed samples were utilized as the working sample; the Ag/AgCl and the platinum wire were used as the reference and counter electrode, respectively. Cyclic voltammetric (CV) was organized in a window of 0-0.47 V at scans of 5-60 mV s^{-1}. Electrochemical impedance spectroscopes (EIS) were measured within a frequency range of 10^5-10^{-2} Hz. Galvanostatic charge-discharges (GCD) preparations are detected at various current density values in a window of 0-0.35 V. As to developed samples, the specific capacitance (C_S) was calculated from the plots of GCD through the equations following [29-31]:

$$C_S=(I{\cdot}\Delta t)/(\Delta V{\cdot}m) \quad (1)$$

where, Δt (s), I (A), ΔV (V), and m (g) are the discharging time, the charge-discharge current, the maximum potential window to discharge the cell, and the mass of working samples, respectively.

RESULTS AND DISCUSSION

1. Material Characterization

The structured procedures of the unique constructions of Na-doped MoS_2 nanosheet on Ni foam are displayed in Fig. 1. Ni foam was selected as the sample substrate due to its great porosity, specific area, and electrical kinetics. The synthesis reactions mainly comprise two steps. Initially, the MoS_2 nanoparticles array was developed straightly on Ni foam through the more accessible hydrothermal technique. After the MoS_2 precursors were utilized as the substrates, sodium nitrate dope was included, and Na-dope particles are significant forms on the area of the MoS_2 nanoparticles array by hydrothermal process, from hierarchical construction Na-doped MoS_2 nanosheet.

The micro-morphologies of MoS_2 and Na-doped MoS_2 nanosheets were analyzed through SEM and TEM. Fig. 2(a) depicts the SEM images of MoS_2 nanoparticles demonstrating the particles and sheet-typed shapes. Fig. 2(b) displays the SEM images of the as-grown Na-doped MoS_2 nanosheet, showing sheet-type nanostructures. Mainly in the Na-doped MoS_2 nanosheet, overlapping the Na-doped particles would confirm a mutual connecting conducted network, making the easiest fast electronic transport in elec-

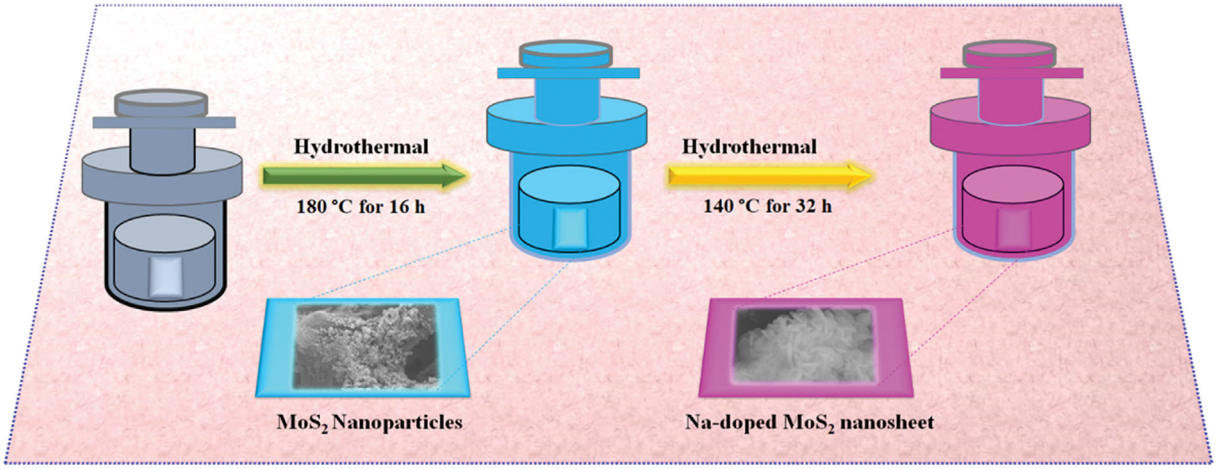

Fig. 1. Schematic diagram illustrating the preparation of MoS_2 electrode and Na-doped MoS_2 nanosheet composites on Ni foam substrate.

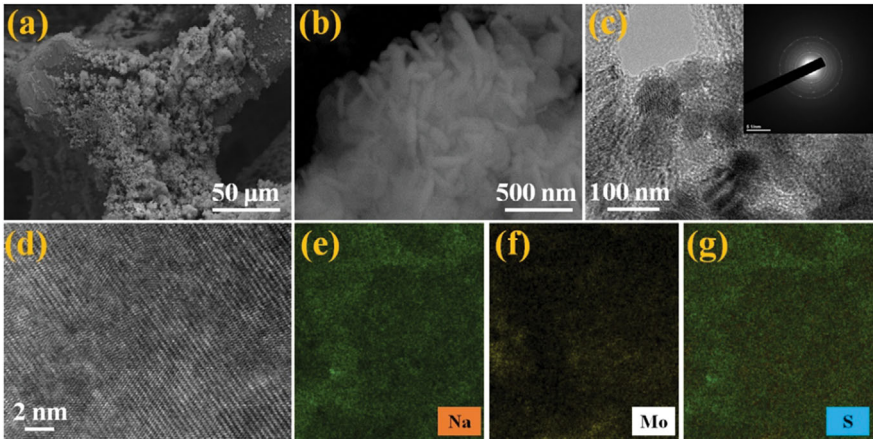

Fig. 2. ((a) and (b)) SEM and FESEM images of pristine MoS_2 nanoparticles and Na-doped MoS_2 nanosheet, ((c) and (d)) TEM and HRTEM images of the pristine MoS_2 nanoparticles and Na-doped MoS_2 nanosheet, and ((e)-(g)) the elemental mapping images of Na-doped MoS_2 nanosheet.

trolyte proceedings. Nevertheless, these Na-doped MoS_2 nanosheet arrays were also improving the stability of the Na-doped MoS_2 because of their superstrength of Na-doped. The Na-doped and MoS_2 were diluted well in DI water through vigorous shaking, providing homogeneous black precursors, which were favored to improve the surface area of the composited materials.

Fig. 2(c) illustrates the representative TEM images of the designed MoS_2, which display the layering platelet. Fig. 2(d) depicts the HRTEM image of the Na-doped MoS_2 nanosheet. The HRTEM manifests usual trends with the particles of MoS_2 mesoporous embedded in Na-doping. The black striped-colored MoS_2 particle layering was identified and appeared to be in devoted contact with the Na-doped layer, which indicates the Na-doped MoS_2 nanosheet visible so that the interlayer spaces among the MoS_2 particles in the nanocomposites were approximated to be 0.72 nm. The EDS patterns of the Na-doped MoS_2 nanosheet are illustrated in Fig. 2(e)-(g). The EDS demonstrates elements of Na, Mo, and S. Thus, it is further evidence that the design of the Na-doped MoS_2 nanosheet was successful.

Fig. 3 demonstrates the XRD analyzer of Na-doped MoS_2 nanosheet. For Na-doped MoS_2 nanosheet, the existence of (002), (100), and (110) angles reveals few-layering nanostructures for MoS_2

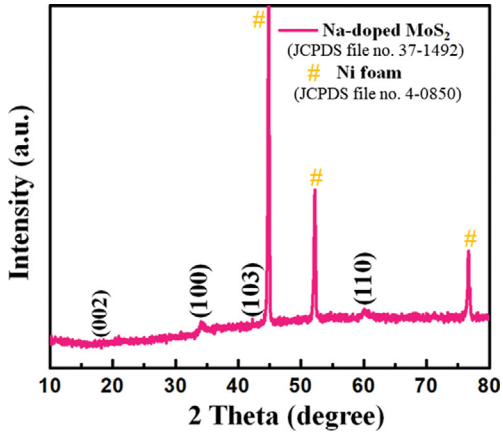

Fig. 3. XRD patterns of pristine MoS_2 nanoparticles electrode and Na-doped MoS_2 nanosheet.

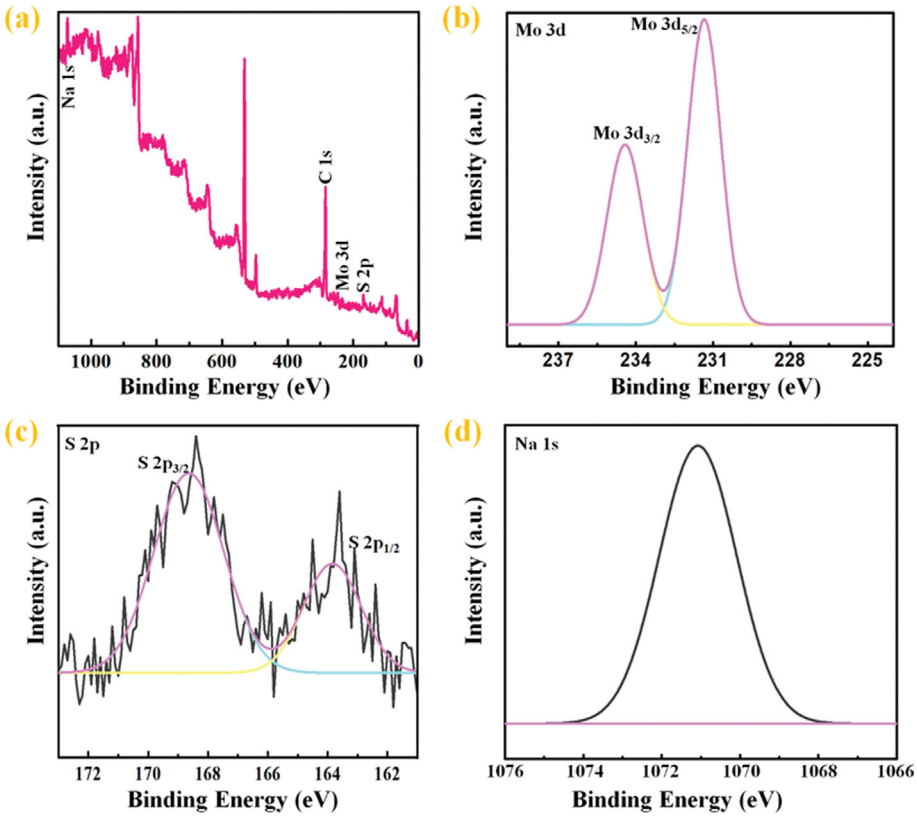

Fig. 4. (a) XPS survey spectra, and (b)-(d) Mo 3d, S 2p, and Na 1S spectra for Na-doped MoS_2 nanosheets.

(JCPDS#37-1492). The diffraction peaks are visibly weaker, suggesting the poorer crystallinity of MoS_2. This was corresponding to the inclusion of the Na-doped hindering the development of the MoS_2 layered crystals during the hydrothermal reactions. Especially, the pattern of XRD manifests that Na-doped MoS_2 sheets are single-phased and have no other angles of Na and Na-components. These outcomes are evidence that Na ions are incorporated into the MoS_2 lattice substituting the Mo ions.

To further investigate, the elemental states and valence compositions of the Na-doped MoS_2 nanosheet composites using the XPS patterns were employed. The XPS analyzer of the Na-doped MoS_2 nanosheet (Fig. 4(a)) illustrates Mo, S, and Na elements. The element of 'C' is formed by surface contaminations. Fig. 4(b) depicts the Mo spectra consisting of Mo $3d_{5/2}$ at 231.79 eV and Mo $3d_{3/2}$ at 234.89 eV. The energy variation among the two phases was 3.1 eV, revealing Mo^{+6} [32,33]. Fig. 4(c) illustrates the S 2p spectra, which possess two peaks at 162.37 eV and 163.49 eV, well-matched S $2p_{3/2}$ and S $2p_{1/2}$, respectively; both peaks are correlated with S^{2-}, and a proven satellite angle at 168.27 eV visible, practicably due to its fraction oxidations of the sulfurs [34]. The electrochemical oxidation of Na 1s was initiated, leading to the 'Na' with a binding energy of approximately 1,071.5 eV, as shown in Fig. 4(d). Therefore, the XPS results indicated that Na^+ was intercalated into MoS_2, which confirmed the successful fabrication of Na-doped MoS_2 nanosheets using the electro-oxidational method.

3-2. Electrochemical Performance in a 3-Electrode Test System

Employing CV, GCD, and EIS tests, we compared electrochemical activity among the designed electrode samples. Fig. 5(a) displays the consequences of CV plots discussing the Ni foam, MoS_2, and Na-doped MoS_2 samples at 5 mV s^{-1}. All samples disclose Faradic peaks due to their redox procedures among the hydroxide ions/metal ions, demonstrating the redox pseudocapacitive (PC) characterizations. The regions in the CV plots of the Na-doped MoS_2 nanosheet electrode were gradually higher than the other Ni foam and MoS_2 nanoparticles electrodes were the greatest. The outcomes reveal that the Na-doped MoS_2 nanosheet composite as the sample possesses superior specific capacity when comparable with Ni foam and pristine MoS_2 samples, demonstrating the successful hydrothermal reactions in the MoS_2 electrode sample through the initiations of Na-dopant. Therefore, the initiation of Na-dopant increases the electrochemically specific region and active sites, thereby increasing the conductivity of the MoS_2. Fig. 5(b) discloses GCD analysis of the as-developed Ni foam, MoS_2, and Na-doped MoS_2 samples in a voltage range of 0-0.35 V at 1 A g^{-1}. Samples both consist of a clear GCD-specific area, further evidencing that all sample electrodes were redox PC electrodes. The plots of all samples possess apparent symmetric features demonstrating that all samples were well-stabilized redox reactions. The Na-doped MoS_2 nanosheet composite has a more expanded discharge time than the MoS_2 and would be storing more charges, indicating that the Na-doped MoS_2 nanosheet has superior specific capacity than the pristine MoS_2 samples. The dominant reason for this phenomenon was the adjustments of the substance morphologies.

Fig. 5(c) shows CV plots of the Na-doped MoS_2 nanosheet at 5,

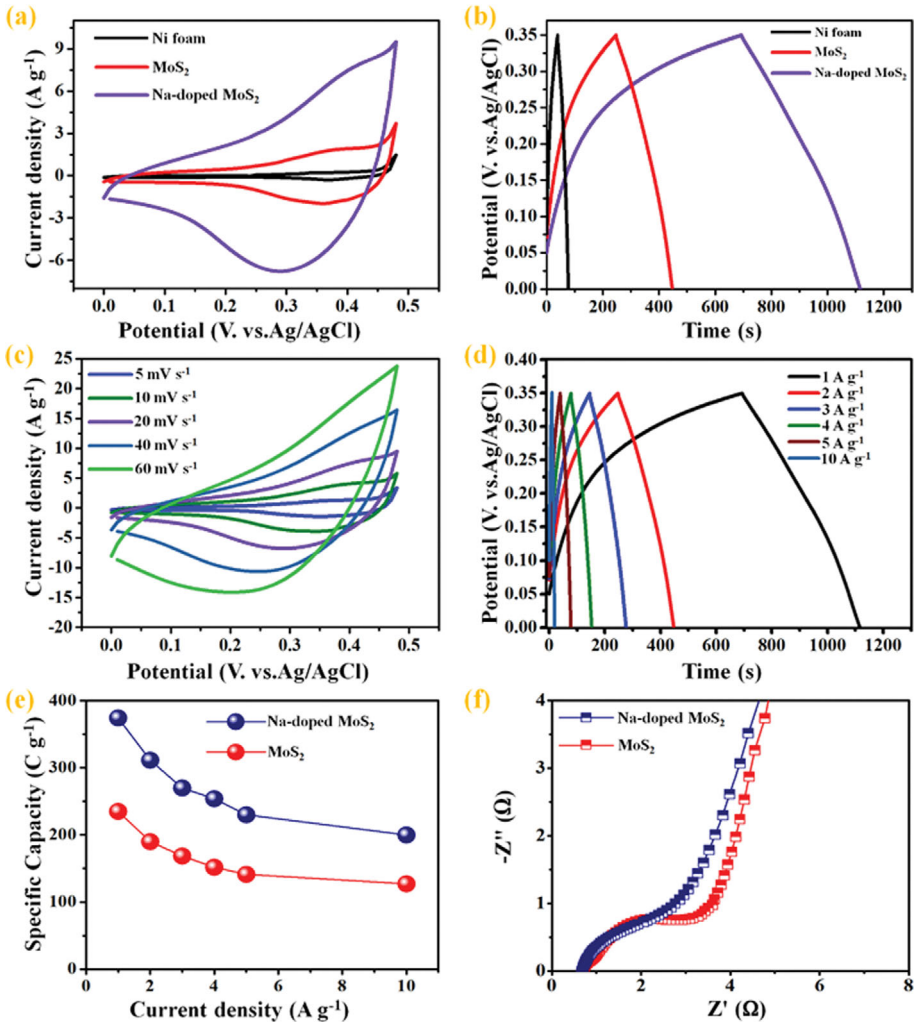

Fig. 5. (a) Comparative CV curves at 5 mV s^{-1} of the Ni foam, MoS_2, and Na-doped MoS_2 electrodes. (b) GCD curves at 1 A g^{-1} of the Ni foam, MoS_2, and Na-doped MoS_2 electrodes. (c) CV curves at different scan rates of the Na-doped MoS_2 nanosheet electrode. (d) GCD curves at different current densities of the Na-doped MoS_2 nanosheet electrode. (e) Specific capacity results of the MoS_2 and Na-doped MoS_2 electrodes at different current densities. (f) Nyquist plots of the MoS_2 and Na-doped MoS_2 electrodes.

10, 20, 30, 40, and 60 mV s^{-1}. CV plots both manifest Faradic peaks, revealing PCs behavior of the Na-doped MoS_2 nanosheet electrode. With rising scans, the oxidational peaks of CV curves also increase direction greater potentials, and reduction peaks rise towards low voltage ranges, respectively [35]. The shapes of these CV plots persisted undamaged at lower scanning rates, revealing the excellent reversibility of the Na-doped MoS_2 nanosheet. Notably, the scans increase, and the redox reactions provide shorter diffusion paths for electrons in the electrolytes that were inadequate to fully pass the sample and reaction with it to supply polarizations, leading to declines in the usage speeds of the electrode samples and a decrease in the capacities [36].

Fig. 5(d) shows GCD plots of the Na-doped MoS_2 nanosheet sample in a voltage range of 0-0.35 V at current densities of 1, 2, 3, 4, 5, and 10 A g^{-1}. These plots possess an apparent platform area, manifesting that the Na-doped MoS_2 nanosheet achieves battery-kind capacitance characteristics at varied current values. In Eq. (1), the specific capacities of the Na-doped MoS_2 nanosheet composite electrodes were 374.3, 311.4, 270, 254, 230, and 200 C g^{-1} at 1, 2, 3, 4, 5, and 10 A g^{-1}, respectively. The GCD plots were almost consistently symmetrical in current values of 1-10 A g^{-1}, disclosing that the GCD procedures have greater coulombic efficiencies. The specific capacities of the Na-doped MoS_2 nanosheet electrode were compared with recently reported similar electrode materials in Table 1.

Fig. 5(e) shows the specific capacities of the developed sample materials at varied current values. The specific capacity of the Na-doped MoS_2 nanosheet electrode was more enlarged than other MoS_2 electrodes. The outstanding specific capacities of the Na-doped MoS_2 nanosheet composite electrode were ascribed to the initiation of the Na-dopant that improved more effective intercontact region and electrical kinetics. The bigger specific areas supply many active sites, while GCD storing enhances spacing utilizations and favors electrolyte penetration. Nevertheless, the Na-doped arrays protect the internal constructions of MoS_2 particles, enhancing stability and efficiently improving the energy-storing Na-doped MoS_2 nanosheet performance.

Table 1. Comparison of the specific capacitance of the Na-doped MoS_2 nanosheet composites electrode prepared in the present work and other reports in the literature

Electrode materials	Preparation method	Specific capacity/ capacitance	Current density	Retention	Ref.
MoS_2-Cs	Hydrothermal	411 F g^{-1}	1 A g^{-1}	93.2% after 1000 cycles	39
MoS_2-graphene	Hydrothermal	243 F g^{-1}	1 A g^{-1}	93.3% after 1000 cycles	40
MoS_2-RGO	MAH	265 F g^{-1}	1 A g^{-1}	92% after 1000 cycles	41
MoS_2-PPY	Hydrothermal	553.7 F g^{-1}	1 A g^{-1}	90% after 500 cycles at 1 A g^{-1}	25
MoS_2-PANI	Exfoliated MoS_2+ polymerization	390 F g^{-1}	4 mA cm^{-2}	86% after 1000 cycles	42
MoS_2-VGVNF	MAH	248 F g^{-1}	5 mV s^{-1}	96% after 1000 cycles	43
MoS_2-NDG	Hydrothermal	245 F g^{-1}	0.25 A g^{-1}	91.3% after 1000 cycles	44
Na-doped MoS_2 nanosheets	Hydrothermal	374.3 C g^{-1}	1 A g^{-1}	87.4% after 5000 cycles	This work

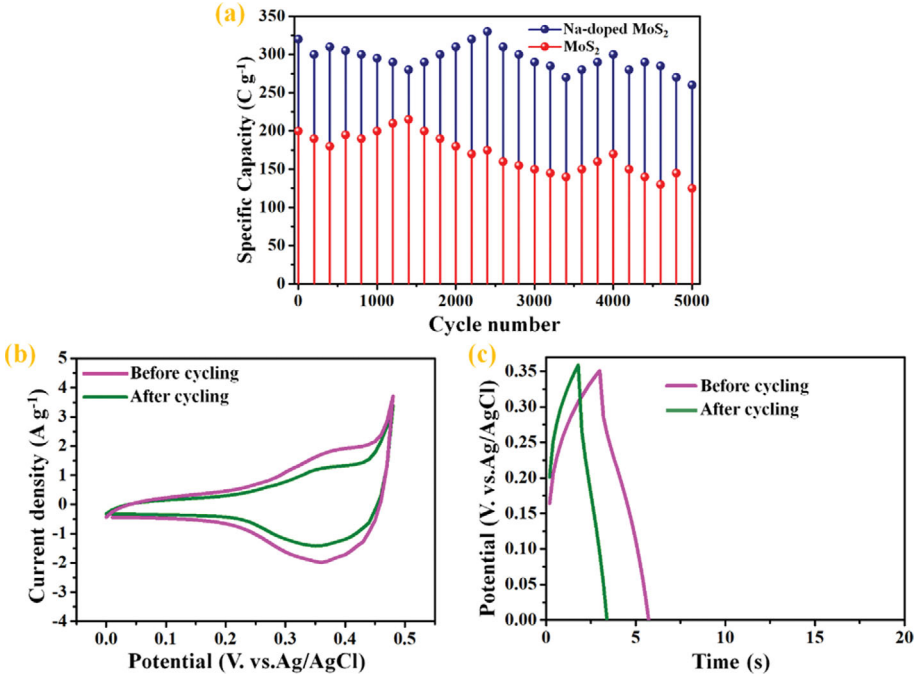

Fig. 6. (a) Cycling performance of Na-doped MoS_2 nanosheet electrode at 5 A g^{-1} after 5000 cycling tests. ((b) and (c)) CV and CD tests before and after cycling tests after 5000 long cycles.

The electrochemical properties of the MoS_2 and Na-doped MoS_2 electrodes were further analyzed for EIS patterns in frequency ranges of 10^{-2}-10^5 Hz with an amplitude of 10 mV. With the reduction in impedance plot frequencies, the EIS curves would be roughly split into three components in Fig. 5(f). The first was the equivalent series resistances (R_s) of the Nyquist plot constituted through the real axis interceptions. The second was the semicircle diameters considering the charge transfer resistances (R_{ct}) structured through electron diffusions. The third was a direct line that represents the ion's diffusional resistances (W) at redox arises. The EIS plots consider the ions diffusions, visualized as the slopes of the plots [37-39]. By calculating the equivalent circuits, the Na-doped MoS_2 nanosheet electrode displays smaller intersections with a real axis and smaller semicircles at higher frequency data; the R_s (0.56 Ω), as well as R_{ct} (2.83 Ω) of the Na-doped MoS_2 nanosheet sample, was lower than another MoS_2 nanoparticles electrode (R_s=0.68 Ω, R_{ct}=5.93 Ω), and the Na-doped MoS_2 nanosheet was smaller. This finding reveals that the unique structure of Na-dopant and MoS_2 nanoparticles assists in improving the conductivity of the sample and favors ultra-charging transmissions. Moreover, the linear slopes of the Na-doped MoS_2 nanosheet were greater than that of the MoS_2 nanoparticles electrode, signifying that the ion diffusion resistances of the Na-doped MoS_2 nanosheet were small; this outcome further discloses that the Na-doped MoS_2 nanosheet demonstrates better electrochemical activity.

Fig. 6(a) demonstrates the cycling activity of the Na-doped MoS_2 nanosheet electrode that was analyzed at 3 A g^{-1} with capacity retentions of 87.4% over 5,000 cycle counts. While testing, the Na-

doped MoS_2 nanosheet composite cycling performances were relatively stable, evidencing that the Na-doped MoS_2 nanosheet possesses better stability. The capacity retention upon energy-storing stability and greater capacity of the composite electrodes was ascribed to the flexibility of Na-dopant in the Na-doped MoS_2 nanosheet. The Na-dopant can not only form open space structures to enhance the interconnections among the working sample and electrolyte and produce full utilizes of electrochemical activeness MoS_2 during the GCD procedures, but also enhance the electrical conductivity of the overall electrodes due to the greater conductivity of Na-dopant. Figs. 6(b) and (c) display CV and CD tests before and after cycling stability tests. These results indicate that the Na-doped MoS_2 nanosheet electrode exhibits excellent cycling stability and is a promising material for commercial energy storage devices.

CONCLUSIONS

We utilized a versatile, simpler hydrothermal method to prepare layer-structured Na-doped MoS_2 nanosheets grown on Ni foam, demonstrating superior performance to the pristine components. The unique structure gradually enlarges the specific region, providing numerous active sites. Introducing Na-dopant enhances the kinetics of the MoS_2 particles and significantly improves charge transport. At 1 A g^{-1}, the highest specific capacity was 374.3 C g^{-1}, compared to 235 C g^{-1} for MoS_2. Integrating Na-dopant into the main nanosheet offers a larger surface area for loading MoS_2 nanoparticles, facilitating easier access for both ion and charge transport in every part of the electrodes. Additionally, the capacity retention remained around 87.4% of the initial capacity after 5000 long cycles. These findings suggest that the Na-doped MoS_2 nanosheet composites hold great promise as suitable electrode materials for high-performance SCs.

ACKNOWLEDGEMENTS

This research was supported by the National Research Foundation of Korea (NRF) grant (2021M3H4A1A02042952) and the Ministry of Education (NRF2021R1A6A1A03039981).

CRediT AUTHORSHIP CONTRIBUTION STATEMENT

Y. A. Kumar: Writing-original draft, Conceptualization, Writing-review, Methodology. **D. K. Kulurumotlakatla**: Data curation, Resources, Investigation, Formal analysis, Writing-review, Methodology, **I.-K. Park**: Supervision, Resources, Project administration, editing, Funding acquisition.

DECLARATION OF COMPETING INTEREST

The authors declare that they have no known competing financial interests or personal relationships that could have appeared to influence the work reported in this paper.

SUPPORTING INFORMATION

Additional information as noted in the text. This information is available via the Internet at http://www.springer.com/chemistry/journal/11814.

REFERENCES

1. C. Xiong, C. Zheng, B. Li and Y. Ni, *Ind. Crops Prod.*, **178**, 114565 (2022).
2. Y. A. Kumar, S. Sambasivam, S. Ahmed Hira, K. Zeb, W. Uddin, T. N. V. Krishna, K. Dasha Kumar, I. M. Obaidat and H.-J. Kim, *Electrochim. Acta*, **364**, 137318 (2020).
3. Y. A. Kumar and H.-J. Kim, *Dalton Trans.*, **47**, 15545 (2018).
4. Y. A. Kumar, T. Anitha and H.-J. Kim, *Energies*, **12**, 1143 (2019).
5. K. Hyun, M. Shin and Y. Kwon, *Korean J. Chem. Eng.*, **39**, 3315 (2022).
6. S. H. Baek, Y. M. Jeong, D. Y. Kim and I. K. Park, *Chem. Eng. J.*, **393**, 124713 (2020).
7. S. Wang, Z.-S. Wu, F. Zhou, X. Shi, S. Zheng, J. Qin, H. Xiao, C. Sun and X. Bao, *Npj Mater. Appl.*, **2**, 7 (2018).
8. H. S. Chang, B.-M. Lee, J. M. Yun and J.-H. Choi, *Korean J. Chem. Eng.*, **39**, 1232 (2022).
9. A. Dang, Y. Sun, Y. Liu, Y. Xia, X. Liu, Y. Gao, S. Wu, T. Li, A. Zada and F. Ye, *ACS Appl. Energy Mater.*, **5**, 9158 (2022).
10. M. F. El-Kady, Y. Shao and R. B. Kaner, *Nat. Rev. Mater.*, **1**, 16033 (2016).
11. Q. Guo, B. Li, M. Shen, W. Li, Q. Gao and G. Xu, *Korean J. Chem. Eng.*, **40**, 1331 (2023).
12. M. H. Gomaa, Z. A. Hamid, M. A. M. Ibrahim, R. A. E. Sttar and E. H. El-Mosallamy, *Korean J. Chem. Eng.*, **40**, 1186 (2023).
13. C. Cao, X. Xie, Y. Zeng, S. Shi, G. Wang, L. Yang, C. Z. Wang and S. Lin, *Nano Energy*, **61**, 550 (2019).
14. J. I. Sohn, Y.-I. Jung, S.-H. Baek, S. N. Cha, J. E. Jang, C.-H. Cho, J. H. Kim, J. M. Kim and I.-K. Park, *Nanoscale*, **6**, 2046 (2014).
15. K.-H. Kim, Y.-J. Song and H.-J. Ahn, *Korean J. Chem. Eng.*, **40**, 1071 (2023).
16. D. Akcan, A. Gungor and L. Arda, *J. Mol. Struct.*, **1161**, 299 (2018).
17. Z. Ye, T. Wang, S. Wu, X. Ji and Q. Zhang, *J. Alloys Compd.*, **690**, 189 (2017).
18. H. Yuan and M. Xu, *Ceram. Int.*, **44**, 15531 (2018).
19. L. W. Wang, F. Wu, D. X. Tian, W. J. Li, L. Fang, C. Y. Kong and M. Zhou, *J. Alloys Compd.*, **623**, 367 (2015).
20. Y. F. Lu, K. W. Wu, Y. J. Zeng, Z. Z. Ye, J. Y. Huang, L. P. Zhu and B. H. Zhao, *Chem. Phys. Lett.*, **582**, 82 (2013).
21. J. Chen, N. Kuriyama, H. Yuan, H. T. Takeshita and T. Sakai, *J. Am. Chem. Soc.*, **123**, 11813 (2001).
22. S. J. Ding, J. S. Chen and X. W. Lou, *Chem. Eur. J.*, **17**, 13142 (2011).
23. M. Y. Sun, J. Adjaye and A. E. Nelson, *Appl. Catal. A*, **263**, 131 (2004).
24. H. S. S. Ramakrishna Matte, A. Gomathi, A. K. Manna, D. J. Late, R. Datta and S. K. Pati, *Angew. Chem. Int. Ed.*, **49**, 4059 (2010).
25. G. F. Ma, H. Peng, J. J. Mu, H. H. Huang, X. Z. Zhou and Z. Q. Lei, *J. Power Sources*, **229**, 72 (2013).
26. N. Zheng, X. Bu and P. Feng, *Nature*, **426**, 428 (2003).
27. J. Xiao, D. Choi, L. Cosimbescu, P. Koech, J. Liu and J. P. Lemmon, *Chem. Mater.*, **22**, 4522 (2010).
28. J. M. Soon and K. P. Loh, *Electrochem. Solid-State Lett.*, **10**, A250 (2007).
29. D. K. Kulurumotlakatla, A. K. Yedluri and H.-J. Kim, *J. Energy Stor.*,

31, 101619 (2020).
30. H. M. Arbi, A. A. Yadav, A. K. Yedluri, M. Moniruzzaman, S. Alzahmi and I. M. Obaidat, *Nanomaterials*, **12**, 3982 (2022).
31. M. Moniruzzaman, A. K. Yedluri, M. R. Pallavolu, H. M. Arbi, S. Alzahmi and I. M. Obaidat, *Nanomaterials*, **12**, 3187 (2022).
32. S. Chen, S. Cui, S. Chandrasekaran, C. Ke, Z. Li, P. Chen, C. Zhang and Y. Jiang, *Electrochim. Acta*, **341**, 135893 (2020).
33. Z. Guo, Y. Wang, M. Li, S. Wang and F. Du, *J. Alloys Compd.*, **832**, 155012 (2020).
34. Z. Yu, N. Zhang, G. Li, L. Ma, T. Li, Z. Tong, Y. Li and K. Wang, *J. Energy Storage*, **51**, 104511 (2022).
35. S. D. Kharade, N. B. Pawar, K. V. Khot, P. B. Patil, S. S. Mali, C. K. Hong, P. S. Patil and P. N. Bhosale, *RSC Adv.*, **6**, 24985 (2016).
36. S. Alipour and M. Arvand, *Colloids Surf. A Physicochem. Eng. Asp.*, **606**, 125456 (2020).
37. H. Zhang, X. Zhang, D. Zhang, X. Sun, H. Lin, C. Wang and Y. Ma, *J. Phys. Chem. B*, **117**, 1616 (2013).
38. A. Wang, M. Zhang, Z. Huang, H. Liu, Z. Wang, Z. Song, W. Zhou, G. Zhu and S. Shao, *J. Solid State Chem.*, **307**, 122760 (2022).
39. S. C. Zhang, R. R. Hu, P. Dai, X. X. Yu, Z. L. Ding, M. Z. Wu, G. Li, Y. Q. Ma and C. J. Tu, *Appl. Surf. Sci.*, **396**, 994 (2017).
40. K. J. Huang, L. Wang, Y. J. Liu, Y. M. Liu, H. B. Wang, T. Gan and L. L. Wang, *Int. J. Hydrogen Energy*, **38**, 14027 (2013).
41. E. G. da Silveira Firmiano, A. C. Rabelo, C. J. Dalmaschio, A. N. Pinheiro, E. C. Pereira, W. H. Schreiner and E. R. Leite, *Adv. Energy Mater.*, **4**, 1301380 (2014).
42. J. Wang, Z. C. Wu, K. H. Hu, X. Y. Chen and H. B. Yin, *J. Alloys Comp.*, **619**, 38 (2015).
43. F. N. I. Sari and J. M. Ting, *Sci. Rep.*, **7**, 5999 (2017).
44. B. Q. Xie, Y. Chen, M. Y. Yu, T. Sun, L. H. Lu, T. Xie, Y. Zhang and Y. C Wu, *Carbon*, **99**, 35 (2016).

Supporting Information

Interface engineering for enhancing the performance of novel sodium-doped MoS_2 nanocomposite: Synthesis and characterization functioning as a high-performance supercapacitor

Yedluri Anil Kumar*, Dasha Kumar Kulurumotlakatla, and Il-Kyu Park***,†**

*Department of Chemical & Petroleum Engineering, United Arab Emirates University (UAEU), Al Ain 15551, United Arab Emirates
**Graduate School of Convergence Science, Pusan National University, San 30 Jangjeon-dong, Geumjeong-gu, Busan 46241, Korea
***Department of Materials Science and Engineering, Seoul National University of Science and Technology, Seoul 01811, Korea
(*Received 1 August 2023 • Revised 15 August 2023 • Accepted 18 August 2023*)

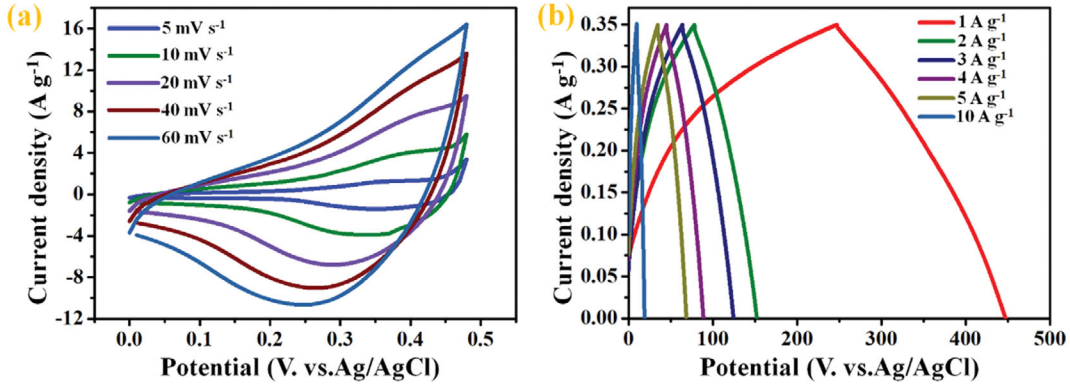

Fig. S1. CV curves and CD plots of pristine MoS_2 nanoparticles electrode at various scan rates and different current densities grown on Ni foam.